npj | advanced manufacturing

Article

Article in Press

https://doi.org/10.1038/s44334-026-00111-x

Additive manufacturing of lunar regolith for reconfigurable building blocks toward lunar habitation

Check for updates

Cole McCallum[1], Youwen Liang[1], Nahid Tushar[1], Ben Xu[2], Bo Zhao[2], Hao Zeng[3] & Wan Shou[1] ✉

Utilizing locally available materials is a crucial step towards sustainable planetary habitation. Lunar regolith has gained tremendous interest in additive manufacturing in the past decades. However, due to the constrained manufacturing facilities and materials on the moon, many existing additive manufacturing methods are not suitable for practical on-site manufacturing. Here, we envision that light-based direct sintering of lunar regolith without a binder can be a feasible approach. Instead of directly manufacturing large structures, we hypothesize that small-scale, reconfigurable building blocks can be an alternative form to construct large and complex structures. To verify the feasibility, we conducted laser sintering of lunar regolith simulants as a proof of concept. Different laser processing parameters were investigated for both individual sintered layers and thicker, multi-layer parts to obtain controllable lunar regolith sintering in three dimensions. We further designed Lego-like interlocking bricks that are reconfigurable for different structure assemblies without additional joining material. Compressive strength and porosity of sintered cubic blocks were evaluated, showing a peak strength of about 3.4 MPa. We hope this work will inspire other in-space manufacturing techniques and enable low-cost space habitation.

Since the first Apollo missions in the late 1960s, establishing a semi-permanent or permanent manned colony on the lunar surface has been subject to rigorous study and exploration. One of the most severe limitations of lunar colonization is the high cost of transporting structures and materials from Earth, highlighting a critical need for onsite manufacturing in space, exploiting local resources[1,2]. Recently, additive manufacturing (AM, a.k.a. 3D Printing) technologies have been considered promising to realize complex solid structure construction with minimal material waste and post-processing work[3,4]. Thus, various AM techniques have been actively studied for potential on-site construction on the Moon[5–7], using local resources such as lunar dust and regolith. Nieke et al. demonstrated aerosol deposition of lunar regolith simulant (EAC-1) into thick films[8]. Fateri and Gebhardt reported selective laser melting (SLM) of lunar regolith[9], and decent 3D structures and parts were demonstrated. Thermoplastic powders were also added and sintered together with simulants as binders to enhance the strength[10,11]. Extrusion-based 3D printing methods are also reported to manufacture structures using lunar regolith[12–14], which may be followed by sintering; however, additional polymer binder and solvents are used to prepare the ink, which might be challenging in space. Vat photo-polymerization approach was also reported using lunar regolith simulant paste for AM[15,16]; however, the addition of polymers and preparation of paste make the adoption for in-space manufacturing unrealistic. Among various AM approaches, it is believed that light-based sintering is one of the most promising strategies, as solar energy is consistently present in great abundance, which can be concentrated directly for heating or used indirectly to power a laser through electricity. Based on this assumption, researchers have also developed solar 3D printing, where simulated sunlight is directly utilized and concentrated with optics to sinter lunar regolith[17,18]. It was demonstrated that the manufacture of glass and mirrors from lunar regolith simulant is feasible[19], meaning that a wide variety of critical components can be manufactured on site. Therefore, it is highly possible to use a minimal number of terrestrial components to build a functional light-based 3D printer on the Moon.

While industrial laser-based additive manufacturing systems typically deliver energy densities in the range of 10^9–10^{11} W/m² at the melt pool, the solar flux available on the Moon is approximately 1360 W/m² due to the absence of an atmosphere[20]. By employing optical concentrators such as Fresnel lenses or parabolic mirrors, this flux can be intensified by factors of up to 10,000 times, yielding focused power densities of $1–10 \times 10^6$ W/m²[21]. This falls within the range of solar furnaces on Earth, such as NREL's High-

[1]Department of Mechanical Engineering, University of Arkansas, Fayetteville, AR, USA. [2]Department of Mechanical and Aerospace Engineering, University of Houston, Houston, TX, USA. [3]Faculty of Engineering and Natural Sciences, Tampere University, Tampere, Finland. ✉e-mail: wshou@uark.edu

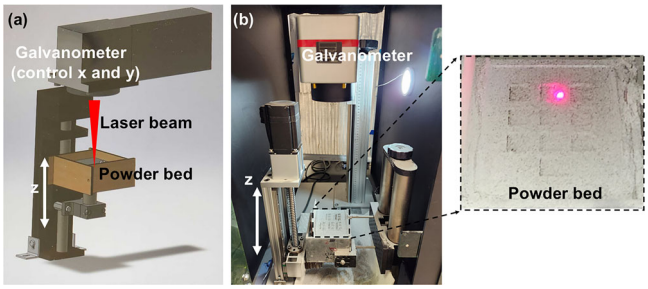


Fig. 1 | Customized selective laser sintering system. a Schematic drawing and **b** photograph.

Flux Solar Furnace, which has achieved focal intensities exceeding 2.5×10^6 W/m² and temperatures above 1800 °C[22]. These levels are sufficient to sinter and even partially melt lunar regolith simulants, as demonstrated in studies where sintering occurred at fluxes of 100–200 kW/m² and temperatures ranging from 900–1200 °C[23,24]. Although this is still orders of magnitude lower than the intensity achieved by high-power lasers, the energy delivered by concentrated solar flux in space is technically adequate for regolith sintering, provided that longer exposure times or slower scan speeds are acceptable.

Although decent progress has been made in utilizing lunar regolith simulants for AM, due to the heterogeneous nature of lunar regolith, various methods were used to prepare these materials for 3D printing. These include sieving powders through a micrometer-scale mesh grids[9], adding thermoplastic polymers as binding agents[10,11], and using solvents or polymer matrices[15,16]. However, these additives and pre-processing inevitably introduce materials that are unavailable or undesirable in the lunar environment, making these approaches unrealistic for in-space manufacturing. A detailed comparison between binder-based and binderless sintering methods reveals key tradeoffs for different applications[25]. Generally, binders can enhance part strength and tolerances[26], but at the cost of requiring significant material transport from Earth. Binderless sintering, on the other hand, demands higher energy input, meaning that the benefits of using 100% in situ resources must be weighed against the need for additional energy collection equipment[24]. Thus, binderless AM without pre-processing represents a more viable approach for ISRU.

Although light-based sintering approaches are widely explored to manufacture lunar regolith parts, directly manufacturing large structural parts with consistent properties remains challenging, due to the complex light-matter interactions and the variability in the composition and shape of regolith[27]. Thus, we hypothesize that developing interconnectable modular structures at a small scale can be an alternative to assembling large parts and structures. Although previous AM work has demonstrated simple brick designs using lunar regolith[17,28,29], a reconfigurable brick structure has not been considered. Buildings on Earth typically use cement to bond bricks; however, simplifying this bonding mechanism is beneficial for the construction of lunar habitation. Therefore, an approach employing a small number of interchangeable, standardized components can be promising for constructing Moon buildings. Inspired by traditional mortise and tenon joints and Lego-like structures for construction[30,31], this research introduces a novel application of direct laser sintering of lunar regolith without binder and pre-processing to create reconfigurable modular bricks aimed for the construction of future lunar habitats.

Results and discussion

Morphology evolution with different laser processing parameters

To understand the influence of laser processing parameters on the raw lunar regolith, a systematic study was conducted using a customized selective laser sintering system (as shown in Fig. 1, details can be found in "Methods" section). Two critical measurements, sintering depth and width, were collected using our defined line pattern (1 × 2.5 mm). While a wide range of parameter combinations were tested, only the combinations that gave a well-defined line were used for measurement. As shown in Fig. 2a, generally, the sintering depth increases with the increase of laser power. Meanwhile, with the decrease in scanning speed, more heat will be accumulated, and the heat-affected zone will also be deeper. While our designed sinter width was 1 mm, the resulting sinters were always wider, as shown in Fig. 2b. However, due to the irregular shape and size distribution of the unprocessed lunar regolith used[18], the influence of laser processing parameters on line width is not well-controlled. It should also be noted that uneven melting can also contribute to structure variation. Three different sintering states were identified based on optical microscope observation: partial melting, full melting, and no melting. The well-defined processing window is shadowed in Fig. 2a, b, which gives us free-standing samples for consistent measurement. A set of microscope images is shown in Fig. 2c to show the evolution of the sintered structure with a fixed power of 36 W and different scanning speeds. It can be observed that the surface of the sintered line becomes rough with the increase in speed. This is closely related to the melting or sintering condition, with a higher local energy density, the regolith tends to melt and form a smoother surface; while insufficient energy results in only partial melting and a rough surface[27,32]. The influence of laser areal energy density on penetration depth of single-layer square samples (5 × 5 mm²) was also investigated and showed consistent results (as shown in Figs. S4 and S5).

Based on the results from single-track line and single-layer 2D square samples, multi-layered cylinders were manufactured. A decent linear relationship is observed (Fig. 2d), namely, the sample thickness increases with the number of layers, which ensured that 3D printing was feasible. However, it was also noted that there were some variations from layer to layer, which could be caused by the nonuniform distribution of regolith and different thermal conduction conditions due to the change of thickness. In addition, delamination could be observed when additional layers were added. Overall, it was found that a medium power of 24–50 W and scanning speeds of 12.5–20 mm/s produced decent line and 2D plane sintering. Representative cylinders are displayed in Fig. 2e, showing a clear thickness increase from 1 layer to 9 layers.

Mechanical property evaluation

To determine the use case for binderless sintering, compressive mechanical testing was performed on 10 × 10 × 10 mm³ cubes (Fig. 4a) manufactured using different areal energy density. The corresponding stress-strain curves of the samples manufactured by the highest areal energy density are shown in Fig. 4b. Here, the samples were tested in different directions: the thickness direction (H1–H32), parallel to laser scan direction (S1–S3), and vertical to laser scan direction (V1–V3). The results show that the sample's modulus and ultimate compressive strength were significantly higher when subjected to loads in line with each layer. However, the maximum strength was about 3.4 MPa, which, while comparable to some previous reports[10,18,33], is still not yet suitable for practical application (with a target of no less than 10 MPa)[34]. It was observed that the measured strength in the laser processing plane is 3–4 times the strength in the thickness direction, indicating a high anisotropy of the mechanical property. It was also observed that the compressive strength generally increased with increasing areal energy density (Fig. 3c), although the variability in the measured strength also increased. The nonuniform distribution and random shape of the granular particles may contribute to relatively low strength and a big variation. Also, it should be noted that the granular particles of the simulants cannot be spread across the powder bed as smoothly as spherical powder. Therefore, the sintered structures had a rough surface and heterogeneous porosity, which contributed to relatively low mechanical properties. Although the current mechanical strength is not sufficient for practical applications, further processing optimization and post-processing can significantly enhance the properties[32].

Furthermore, porosity was calculated from micro computed tomography (micro-CT) scans (Fig. 3d, e) with values of about 52.4% and 47.9% for specimens made from 24 W (or 12 J/mm²) and 50 W (or 18 J/mm²), respectively (details of sample fabrication parameters can be found in Table S2). By counting continuous volumes in the micro-CT images, it was

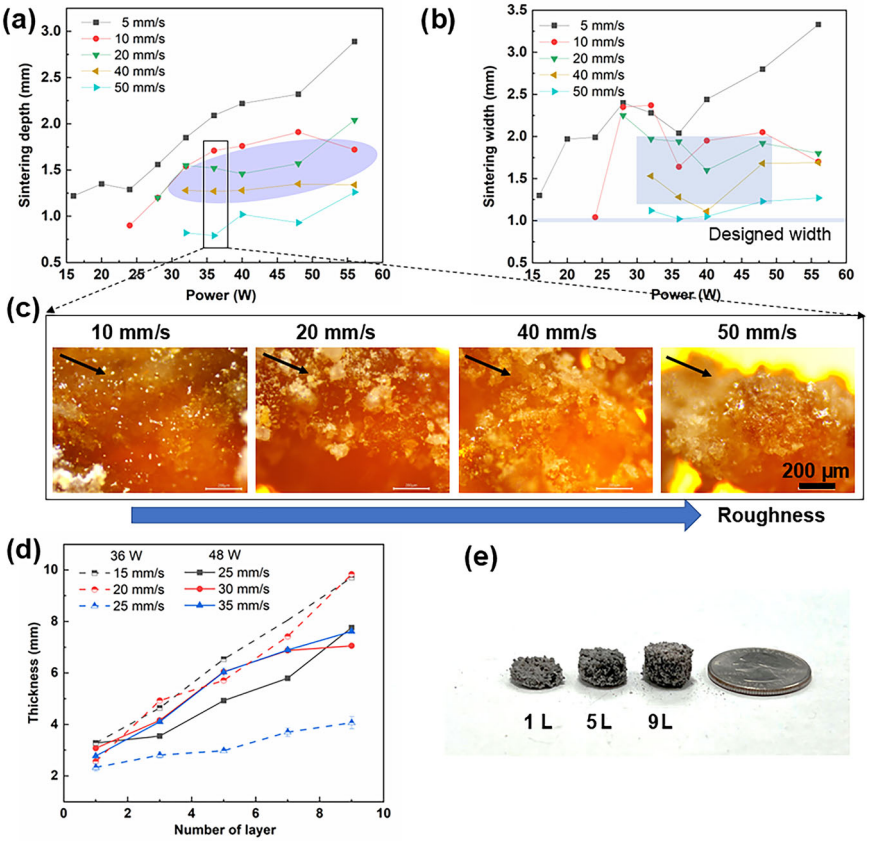


Fig. 2 | Laser processing for structure sintering. **a** Power influence with different scanning speeds on sintering depth. The shadowed area indicates a well-defined sintering window. **b** Power and scanning speed influence on sintering width. **c** Morphology evolution of lunar regolith with different scanning speeds along scan direction indicated by arrow. **d** Laser processing parameters influence on height of circular shapes. **e** Photographs of representative cylinder samples with different layers.

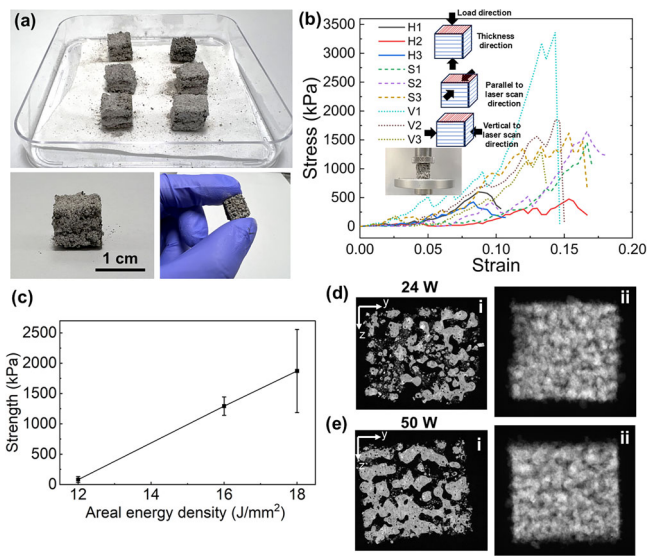


Fig. 3 | Compression test of cubic lunar regolith samples. **a** Photographs of the manufactured test samples. **b** Stress-strain curves of cubic samples measured from different directions. (Samples were fabricated with laser power of 50 W, scanning speed of 20 mm/s and hatch space of 0.25 mm.) **c** Influence of areal energy density on strength. Micro-CT scans of sample made by laser power of **d** 24 W and **e** 50 W: (i) cross section; (ii) average porosity map. (24 W sample corresponds to 12 J/mm^2 and 50 W corresponds to 18 J/mm^2.).

found that the specimen made with 50 W had a lower number of identified objects (namely, less disconnected domains) and a greater mean object volume (or bigger connected domains), suggesting greater cohesion between hatch lines and between layers.

In addition to the porosity obtained using simple thresholding of the CT image, the mixel method[35], which accounts for sub-resolution porosity, found a slight decrease in porosity for both samples. The significant difference in observed compressive strength is most likely a result of this poor bonding, and not the overall porosity, which remained similar between samples. The porosity results obtained in this study are consistent with those reported by Goulas et al.[33], along with a comparable maximum compressive strength of approximately 4.2 MPa. Further melting regolith into a ceramic/glassy state was reported to improve the compressive strength[11,32], but can be challenging for controllable 3D printing. Besides, proper thermal post-treatment can significantly improve the mechanical performance of the additively manufactured lunar regolith structure[32].

Reconfigurable bricks

Interconnectable structures at the centimeter scale were designed and manufactured, as shown in Fig. 4a, with both two-dimensional and three-dimensional features. One structure has an "H" shape, working as the female connection, and the other one has a "+" shape, working as the male connection unit (Fig. 4a-i). More complex connection features (Fig. 4a-ii and iii) were also designed and fabricated for 3D assembly. As a proof-of-concept, we also showed that these modular bricks can be connected to form a self-supporting bridge (Fig. 4b-i) and other simple reconfigurable structures (Fig. 4b-ii), including a wall and a shielding unit. Different from previous selective laser sintering/melting work focused on small parts[9,28], our reconfigurable brick designs can provide an alternative method for building large-scale constructions. Although these structures were at the centimeter scale, we envision that such modular bricks can be interconnected to produce larger structures and constructions. Due to the surface roughness and porosity, the connection realized by our current bricks was not as tight as that of Lego bricks. Yet, with further processing and structure optimization, the construction of complex and seamless habitation using modular bricks without additional materials is possible and promising.

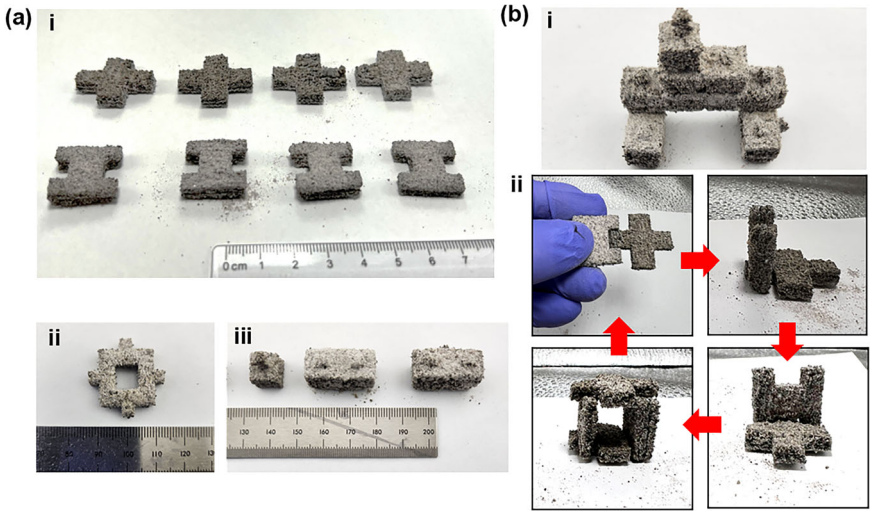


Fig. 4 | Reconfigurable modular bricks. **a** Photographs of bricks with constant (i, ii) and variable (iii) thickness geometry. **b** Proof of concept demonstrations of reconfigurable assembly in (i) one and (ii) multiple directions.

Several challenges were identified during the reconfigurable assembly process. First, surface roughness impeded proper inter-brick contact, leading to insufficient mechanical engagement and tightness; this highlights the need for surface finish optimization to improve connection quality (especially tightness). Second, instances of delamination and structural failure were observed, primarily attributed to non-uniform sintering or partial melting; this underscores the need for a refined thermal processing approach to achieve fully densified and mechanically robust components. Generally, melting is preferred over sintering to obtain denser and smoother structures. Finally, the structural versatility of the current demonstration is limited by the geometry of the two available modular bricks, suggesting that additional brick designs are necessary to enable more complex and adaptable assemblies.

Implications and future work

This work demonstrates a modular manufacturing paradigm for future lunar construction by fabricating reconfigurable building blocks directly from lunar regolith. Compared with directly printing large monolithic structures, the proposed approach offers advantages in manufacturing simplicity, structural repairability, and construction flexibility. Furthermore, the relatively low laser energy density required for binderless sintering, together with the elimination of imported binders and extensive material preprocessing, makes this approach attractive for in-situ resource utilization (ISRU) in lunar and other extraterrestrial environments. Regarding the practical application perspective, the size of the current system is portable, but should be increased for bigger building blocks. Although the fabricated parts exhibit relatively high porosity and moderate mechanical strength, porous regolith components may still be beneficial for lightweight construction, thermal insulation, and radiation shielding. We also envision that concentrated solar energy can be utilized to build a larger and more powerful system for ISRU on the Moon. Assuming proper components, including mechanical and electrical parts with reasonable weights and size, can be transported to the Moon, even if not fully automated, structural materials can be manufactured semi-automatically on the Moon.

Future work should focus on improving both the manufacturing process and the resulting material properties to enable practical lunar deployment. Automated powder spreading, adaptive laser control, and robotic assembly should be integrated to achieve reliable, long-duration autonomous manufacturing. In addition, the feasibility of utilizing concentrated solar energy or solar-powered laser systems should be investigated to further reduce energy requirements on the lunar surface.

From a materials perspective, further optimization of laser processing parameters, scanning strategies, and thermal post-treatment is needed to reduce porosity, strengthen interlayer bonding, and minimize mechanical anisotropy. Finally, experiments under representative lunar conditions, including vacuum, reduced gravity, and extreme thermal cycling, together with optimized interlocking brick geometries and robotic assembly strategies, will be essential for translating this proof-of-concept into a scalable and resilient construction technology for future lunar habitats.

This research serves as proof of concept for future onsite manufacturing of small-scale reconfigurable bricks for large construction assembly, leveraging abundant lunar regolith and light energy. We demonstrated that with moderate laser processing energy density, different modular brick structures can be manufactured, and further assembled and reconfigured to different shapes. Although promising on the reconfigurable aspect, disadvantages were also observed, including delamination and anisotropic properties in the fabricated parts, and low mechanical strength, which require further work to resolve for practical applications. Some key conclusions from this research are as follows.

(1) Under ambient conditions, only a reasonable laser energy density (related to both power and scanning speed) is required to manufacture controllable structures.

(2) The mechanical properties of parts produced via this sintering method are highly anisotropic (the difference can be as high as 4 times). More research is needed to understand this anisotropicity and optimize the mechanical properties along different directions, especially to enhance the interlayer strength.

(3) Surface finish is critical for a seamless connection between different modular bricks.

In spite of the limitations listed above, this research demonstrated the feasibility of reconfigurable modular bricks fabricated from lunar regolith using a light-based sintering without a binder. Future work should be conducted to understand the manufacturing process in a vacuum environment[14,18], as well as the resulting materials in detail. It is envisioned that complex and large structures can be developed using small, reconfigurable modular bricks through ISRU.

Methods

Materials

The exact composition of lunar regolith varies slightly depending on where it is collected; however, samples taken from the Apollo missions across multiple sites consistently contain the compounds SiO_2, Al_2O_3, CaO, MgO, FeO, TiO_2, and MnO in significant quantities[36,37]. The simulant consists of a mixture of silicate minerals with varying ratios of plagioclase, pyroxene, and olivine end members, which together reflect the mineral composition observed from samples across multiple Apollo sites[37]. Among these compounds, SiO_2 is the most abundant, although the other oxides present in regolith contribute about 50 ~ 60% to the overall mass. In this paper, the terms "lunar regolith" and "lunar regolith simulant" are used

Table 1 | Chemical composition of lunar regolith simulant (provided by the vendor)

Oxide	SiO_2	TiO_2	Al_2O_3	FeO	MnO	MgO	CaO	Na_2O	K_2O	P_2O_5	LOI
wt.%	49.12	0.63	26.29	3.20	0.06	2.86	13.52	2.55	0.34	0.17	0.41

interchangeably. It should be noted that all experiments were performed using LHS-1 Lunar Highlands Simulant (provided by Space Resource Technologies), with a specific composition listed in Table 1. The corresponding particle size distribution can be found in the supplementary information, Fig. S1. The regolith simulant had a bulk density of 1.40 g/cm^3 and a tapped density of 1.63 g/cm^3. For lunar regolith and any of its simulants, it cannot be assumed that values such as the density and heat transfer coefficient remain constant, especially at the high temperatures needed for sintering to occur[38]; therefore, it was necessary to experiment with different processing parameters (Fig. S2) to find the conditions under which sintering occurs, but not complete melting of regolith (see trial samples in Fig. S3). Powder was stored in a sealed pouch to prevent moisture from entering the powder before use. In this work, lunar regolith was used as received without any further processing, nor was the bulk composition modified through the addition of other material.

Process and design

A small-scale powder bed was constructed for brick fabrication (Fig. 1). A motorized Z stage was placed under an 80 W fiber laser (wavelength of 1064 nm, OMTech). In-plane motion (x and y) was realized by the galvanometer scanner. The powder container (80×80 mm^2) was built and attached to the adjustable Z-axis stage. The powder bed itself was designed to hold a powder thickness of up to 40 mm. The laser was focused on the surface of the powder bed (aligned with the walls). Powder was deposited at one edge of the powder bed and wiped across the powder surface using a rigid rod. The height was kept level by pressing the rod against the level walls. Based on visual inspection, this method maintained surface flatness to within approximately the particle size scale, with an estimated thickness variation of about 0.1 mm at a confidence level of 75%. This ensured an even surface kept at the laser focal plane. In this study, the laser was fixed at a repetition rate of 4000 kHz, which can be approximated to a continuous wave laser. An atmosphere of 101.2 kPa and a temperature of 21 °C were maintained for this study. More details about energy density calculation and the justification of average laser power can be found in the supplementary information. The printing pattern was designed using LightBurn software, which is essentially a 2D pattern. By moving the Z stage, a 3D structure can be programmed and manufactured.

To determine the processing window for sintering (with partial melting), both 1×2.5 mm^2 line patterns and 5×5 mm^2 square patches were designed and studied (Fig. S4) under various laser processing parameters, including scanning speed and energy density. While different hatch spaces (ranging from 0.01 to 1 mm) were studied, only those between 0.1 and 0.5 mm yielded reasonable sintering. Below 0.1 mm, the penetration depth remained extremely low—even under conditions inducing surface melting—making multilayer structures unattainable with the current setup. Above 0.5 mm, incomplete sintering occurred between adjacent scan tracks. Consequently, hatch spaces of 0.1 mm and 0.25 mm were selected for subsequent experiments. To identify the most promising parameters for binderless printing, a tweezer was used to delicately extract and store samples. The line width was determined by measuring the impression left in the powder bed, while the depth was measured directly from the samples. To precisely determine the penetration depth of the single-layer squares (repeated three times), a method adapted from Murali and Haber was used[39] (see supplementary information for details). To mitigate potential inconsistencies in penetration depth estimation caused by imaging artifacts, additional sintering lines were embedded as calibration references (Fig. S4).

Areal energy density, defined as $E_a = \frac{P}{vh}$ (where P, v, and h correspond to average laser power, scanning speed, and hatch space), was explored primarily through varying the scanning speed and power within ranges 5–50 mm/s and 8–80 W, respectively. The laser spot size was approximately 50 µm. The parameters used for the single-layer sintering study can be found in the supplementary information Table S1. Samples with partial melting and minimal microstructural variation typically had a height along the z-axis ranging from 1.6 to 3.1 mm. Accordingly, sintering parameters that produced samples within this height range were retained for the multilayer sintering study.

To realize additive manufacturing of thicker 3D parts, multi-layer sintering was conducted. Based on our preliminary single-layer study, parameters that induced partial melting were selected for further investigation. To determine the limits of multilayer sintering, circular layers were sintered from regolith with layer counts ranging from 1 to 9. The resulting cylinders were measured to establish the relationship between thickness and the number of layers. To avoid both delamination and excessive melting in multilayer parts, a z-axis layer depth of 1.5 mm was chosen based on the penetration depth results (Fig. S5). Following sintering, the cylinder heights were measured using calipers.

Furthermore, 1 cm^3 (or $10 \times 10 \times 10$ mm^3) cubes were fabricated with different areal energy densities through tuning laser power, scanning speed, and hatch space (with the scanning strategy shown in Fig. S6). Specifically, samples were fabricated with areal energy density of 12 J/mm^2 (24 W, 20 mm/s and 0.1 mm hatch space), 16 J/mm^2 (36 W, 12.5 mm/s and 0.1 mm hatch space) and 18 J/mm^2 (50 W, 20 mm/s, and 0.25 mm hatch space). See Fig. S7 for the stress-strain curves of samples fabricated with laser power of 24 W (or areal energy density of 12 J/mm^2).

After verifying multilayer binderless sintering, the laser parameters (with areal energy density of 16 and 18 J/mm^2) produced decent mechanical properties, which were recorded and used to build more complex structures. A simple two-part building unit (Fig. 4a-i and ii) was designed to work as male and female connectors for 2D or 3D structures. This design carried the advantage that such structures could be built without varying the shape of individual layers, making the sintering process comparatively faster. A second and more complex set of assembly bricks (Fig. 4a-iii) was then created using variable geometry in the thickness direction. These Lego-like structures were fabricated as reconfigurable bricks to test if they could be connected to others to build larger and more complex structures.

Characterizations

Optical images were obtained using a Zeiss microscope with side light illumination. The compressive mechanical test was performed using a Mark 10 tester with an M5-300 force gauge. The loading speed of the tester is 1 mm/min, and the force gauge obtained 10 readings per second. Micro computed tomography (CT) was performed on a Nikon X TH 225 ST µCT system to characterize the porosity of sintered bricks, with a scanning resolution of 9.8 µm. The total scanning time of the 1 cm^3 structure was about 27 min. Porosity measurements were taken using both a thresholding method and a histogram curve fit based on "mixel" porosity[35].

Data availability

The datasets generated and/or analyzed during the current study are not publicly available as they are part of an ongoing study, but are available from the corresponding author on reasonable request.

Received: 4 November 2025; Accepted: 9 August 2026;
Published online: 29 August 2026

References

1. Happel, J. A. Indigenous materials for lunar construction. *Appl. Mech. Rev.* **46**, 313–325 (1993).

2. Isachenkov, M., Chugunov, S., Akhatov, I. & Shishkovsky, I. Regolith-based additive manufacturing for sustainable development of lunar infrastructure – An overview. *Acta Astronaut.* **180**, 650–678 (2021).
3. Tay, Y. W. D. et al. 3D printing trends in building and construction industry: a review. *Virtual Phys. Prototyp.* **12**, 261–276 (2017).
4. El-Sayegh, S., Romdhane, L. & Manjikian, S. A critical review of 3D printing in construction: benefits, challenges, and risks. *Arch. Civ. Mech. Eng.* **20**, 1–25 (2020).
5. Lim, S., Prabhu, V. L., Anand, M. & Taylor, L. A. Extra-terrestrial construction processes – Advancements, opportunities and challenges. *Adv. Space Res.* **60**, 1413–1429 (2017).
6. Sacco, E. & Moon, S. K. Additive manufacturing for space: status and promises. *Int. J. Adv. Manuf. Technol.* **105**, 4123–4146 (2019).
7. Ulubeyli, S. Lunar shelter construction issues: the state-of-the-art towards 3D printing technologies. *Acta Astronaut.* **195**, 318–343 (2022).
8. Nieke, P., Kita, J., Häming, M. & Moos, R. Manufacturing dense thick films of lunar regolith simulant EAC-1 at room temperature. *Materials* **12**, 487 (2019).
9. Fateri, M. & Gebhardt, A. Process parameters development of selective laser melting of lunar regolith for on-site manufacturing applications. *Int. J. Appl. Ceram. Technol.* **12**, 46–52 (2015).
10. Zhao, H. et al. Development of lunar regolith composite and structure via laser-assisted sintering. *Front. Mech. Eng.* **17**, 6 (2022).
11. Indyk, S. J. & Benaroya, H. A structural assessment of unrefined sintered lunar regolith simulant. *Acta Astronaut.* **140**, 517–536 (2017).
12. Jakus, A. E., Koube, K. D., Geisendorfer, N. R. & Shah, R. N. Robust and elastic lunar and martian structures from 3D-printed regolith inks. *Sci. Rep.* **7**, 44931 (2017).
13. Taylor, S. L. et al. Sintering of micro-trusses created by extrusion-3D-printing of lunar regolith inks. *Acta Astronaut.* **143**, 1–8 (2018).
14. Geng, Z. et al. A novel 3D printing scheme for lunar construction with extremely low binder utilization. *Addit. Manuf.* **99**, 104657 (2025).
15. Altun, A. A. et al. Additive manufacturing of lunar regolith structures. *Open Ceram.* **5**, 100058 (2021).
16. Xiao, C. et al. Additive manufacturing of high solid content lunar regolith simulant paste based on vat photopolymerization and the effect of water addition on paste retention properties. *Addit. Manuf.* **71**, 103607 (2023).
17. Meurisse, A., Makaya, A., Willsch, C. & Sperl, M. Solar 3D printing of lunar regolith. *Acta Astronaut.* **152**, 800–810 (2018).
18. Fateri, M., Pitikaris, S. & Sperl, M. Investigation on wetting and melting behavior of lunar regolith simulant for additive manufacturing application. *Microgravity Sci. Technol.* **31**, 161–167 (2019).
19. Schleppi, J. et al. Manufacture of glass and mirrors from lunar regolith simulant. *J. Mater. Sci.* **54**, 3726–3747 (2019).
20. NASA. Moon fact sheet. NASA Space Science Data Coordinated Archive https://nssdc.gsfc.nasa.gov/planetary/factsheet/moonfact.html (2025).
21. Leutz, R. & Suzuki, A. In *Nonimaging Fresnel Lenses: Design and Performance of Solar Concentrators*, 77–99 (Springer, 2001).
22. National Renewable Energy Laboratory. At 30 years young, the future is bright for NREL's high-flux solar furnace. NREL https://www.nrel.gov/csp/facility-hfsf (2020).
23. Biswas, D. *Efficient Sintering of Lunar Soil using Concentrated Sunlight* (The University of Maine, 2023).
24. Gines-Palomares, J.-C. et al. Laser melting manufacturing of large elements of lunar regolith simulant for paving on the Moon. *Sci. Rep.* **13**, 15593 (2023).
25. Azami, M. et al. A comprehensive review of lunar-based manufacturing and construction. *Prog. Aerosp. Sci.* **150**, 101045 (2024).
26. Azami, M., Aubin-Fournier, P.-L. & Skonieczny, K. Enhancing economical lunar-based manufacturing by incorporating lunar regolith into polyether–ether–ketone (PEEK): material development, additive manufacturing, and characterization. *Prog. Addit. Manuf.* **10**, 5675–5681 (2025).
27. Iantaffi, C. et al. Laser additive manufacturing of lunar regolith simulant: new insights from in situ synchrotron X-ray imaging. *Addit. Manuf.* **101**, 104711 (2025).
28. Xu, J. et al. 3D printing of hypothetical brick by selective laser sintering using lunar regolith simulant and ilmenite powders. *Proc. SPIE* **10842**, 1084208 (2019).
29. Fateri, M. et al. Solar sintering for lunar additive manufacturing. *J. Aerosp. Eng.* **32**, 04019101 (2019).
30. Feio, A. O., Lourenço, P. B. & Machado, J. S. Testing and modeling of a traditional timber mortise and tenon joint. *Mater. Struct.* **47**, 213–225 (2014).
31. Barhemat, R., Mahjoubi, S., Li, V. C. & Bao, Y. Lego-inspired reconfigurable modular blocks for automated construction of engineering structures. *Autom. Constr.* **139**, 104323 (2022).
32. Wang, R., Qiao, G. & Song, G. Additive manufacturing by laser powder bed fusion and thermal post-treatment of the lunar-regolith-based glass-ceramics for in-situ resource utilization. *Constr. Build. Mater.* **392**, 132051 (2023).
33. Goulas, A., Binner, J. G., Engstrøm, D. S., Harris, R. A. & Friel, R. J. Mechanical behaviour of additively manufactured lunar regolith simulant components. *Proc. Inst. Mech. Eng. L* **233**, 1629–1644 (2019).
34. Yu, H., Kharel, S., Lau, C. & Ng, K. Development of high-strength and durable coal char-based building bricks. *J. Build. Eng.* **74**, 106908 (2023).
35. Zhuang, L., Shin, H.-S., Yeom, S., Pham, C. N. & Kim, Y.-J. A novel method for estimating subresolution porosity from CT images and its application to homogeneity evaluation of porous media. *Sci. Rep.* **12**, 16229 (2022).
36. Akisheva, Y. & Gourinat, Y. Utilisation of Moon regolith for radiation protection and thermal insulation in permanent lunar habitats. *Appl. Sci.* **11**, 3853 (2021).
37. Sen, S., Ray, C. S. & Reddy, R. G. Processing of lunar soil simulant for space exploration applications. *Mater. Sci. Eng. A* **413-414**, 592–597 (2005).
38. Kost, P.-M. et al. Thermal properties of lunar regolith simulant melting specimen. *Acta Astronaut.* **187**, 429–437 (2021).
39. Murali, S. & Haber, R. A. Microstructural characterization of green ceramic structures using different epoxy infiltration methods. Department of Materials Science and Engineering, Rutgers University.

Acknowledgements

This work was supported by the Honors College Undergraduate Research Grant to C.M. and the Startup Package from the University of Arkansas to W.S.

Author contributions

C.M.: Formal analysis, Investigation, Methodology, Validation, Visualization, Writing-original draft, Writing-review & editing. Y.L.: Formal analysis, Investigation, Writing-review & editing. N.T.: Investigation, Writing-review & editing. B.X.: Methodology, Writing-review & editing. B.Z.: Methodology, Writing-review & editing. H.Z.: Methodology, Visualization, Writing-review & editing. W.S.: Conceptualization, Formal analysis, Methodology, Visualization, Funding acquisition, Resources, Supervision, Writing-original draft, Writing-review & editing. All authors have read the manuscript and approve its publication in this journal.

Competing interest

The authors declare no competing interests.

Additional information

Supplementary information The online version contains supplementary material available at https://doi.org/10.1038/s44334-026-00111-x.

Correspondence and requests for materials should be addressed to Wan Shou.

Reprints and permissions information is available at http://www.nature.com/reprints

Publisher's note Springer Nature remains neutral with regard to jurisdictional claims in published maps and institutional affiliations.

Open Access This article is licensed under a Creative Commons Attribution-NonCommercial-NoDerivatives 4.0 International License, which permits any non-commercial use, sharing, distribution and reproduction in any medium or format, as long as you give appropriate credit to the original author(s) and the source, provide a link to the Creative Commons licence, and indicate if you modified the licensed material. You do not have permission under this licence to share adapted material derived from this article or parts of it. The images or other third party material in this article are included in the article's Creative Commons licence, unless indicated otherwise in a credit line to the material. If material is not included in the article's Creative Commons licence and your intended use is not permitted by statutory regulation or exceeds the permitted use, you will need to obtain permission directly from the copyright holder. To view a copy of this licence, visit http://creativecommons.org/licenses/by-nc-nd/4.0/.

© The Author(s) 2026

This Article in Press is shared early to give you faster access to new research. It is citable and carries a permanent DOI. The final edited version will replace it automatically.